JOURNAL OF THERMOPHYSICS AND HEAT TRANSFER
Vol. 15, No. 3, July–September 2001

Mass-Transfer Distribution in Rotating, Two-Pass, Ribbed Channels with Vortex Generators

V. Eliades,* D. E. Nikitopoulos,† and S. Acharya‡
Louisiana State University, Baton Rouge, Louisiana 70803

Local and global effects of cylindrical vortex generators on the mass-transfer distributions over the four active walls of a square, rib-roughened rotating duct with a sharp 180-deg bend are investigated. Cylindrical vortex generators (rods) are placed above, and parallel to, every other rib on the leading and trailing walls of the duct so that their wake can interact with the shear layer and recirculation region formed behind the ribs, as well as the rotation-generated secondary flows. Local increases in near-wall turbulence intensity resulting from these interactions give rise to local enhancement of mass (heat) transfer. Measurements are presented for duct Reynolds numbers Re in the range 5×10^3–3×10^4 and for rotation numbers in the range 0–0.3. The rib height-to-hydraulic diameter ratio e/Dh is fixed at 0.1, and the rib pitch-to-rib height ratio P/e is 10.5. The vortex generator rods have a diameter-to-rib height ratio d/e of 0.78, and the distance separating them from the ribs relative to the rib height s/e is 0.55. Mass-transfer measurements of naphthalene sublimation have been carried out using an automated acquisition system and are correlated with heat transfer using the heat/mass transfer analogy. The results indicate that the vortex generators tend to enhance overall mass transfer in the duct, compared to the case where only ribs are present, both before and after the bend at high Reynolds and rotation numbers. Local enhancements of up to 30% are observed on all four walls of the duct. At low Reynolds numbers, for example, 5×10^3, the insertion of the rods often leads to mass-transfer degradation. At high Reynolds numbers, for example, 3×10^4, the enhancement due to the rods occurs on the surfaces stabilized by rotation (trailing edge on the inlet pass and leading edge on the outlet pass) and the side walls. The enhancement is more pronounced as the rotation number is increased. The detailed measurements in a ribbed duct with vortex-generator rods clearly show localized regions of enhanced mass (heat) transfer at Reynolds and rotation numbers within the envelope of practical interest for gas-turbine blade cooling applications.

Introduction

ONE of the primary goals in the development of advanced turbine systems is to explore more effective methods of heat removal from the turbine blades. This paper deals with the flow and heat transfer in the internally ribbed coolant channels of a rotating gas turbine blade and aims to examine heat transfer enhancement brought about by placing vortex generators above the ribs in the coolant passages. This expected enhancement is based on observations made in flow past ribs[1] in which it was shown that the separated shear layer behind the rib was characterized by vortical structures and that these structures could be manipulated by introducing an external perturbation into the flow to promote mixing behind the rib. Greater mixing and shear layer growth behind the ribs is expected to lead to enhancement in surface heat transfer. In this paper, the vortex street behind a cylindrical vortex generator mounted above the rib will be used as the external perturbation, and its effect on the heat transfer from the ribbed surface will be examined. The focus is to consider a realistic two-pass ribbed coolant channel geometry and to examine the effect of vortex generators under rotational conditions that are more representative of turbine blade cooling.

Numerous experimental investigations reporting the local and average heat transfer behavior in ribbed channels are available in the literature (e.g., see Refs. 2–7). In general, these studies consistently report significant heat transfer enhancement due to the ribs, with peak heat transfer values in the vicinity of reattachment and just upstream of the rib. Acharya et al.[8] have reported measurements of velocity and heat transfer past a surface mounted rib and have shown the correlation between the surface heat transfer and near-wall velocity fluctuations. Karniadakis et al.[9] performed a numerical study and, using the Reynold's analogy of momentum and heat transfer, showed that heat transfer rate increases with flow instability.

In recent years, more effective heat removal techniques based on manipulating the flow structures in a shear layer or boundary layer have been explored. A half delta wing geometry has been shown to generate longitudinal vortices embedded in the boundary layer in such a way that heat transfer dominates over momentum transfer.[10] With this vortex generator geometry, it was shown that the maximum heat transfer occurred at low Reynolds numbers.[11] A small fencelike geometry placed opposite a ribbed wall was shown to reduce the occurrence of local hot spots in the fully developed region by inducing a more uniform heat transfer distribution.[12] A cylindrical vortex generator placed above and parallel to the ribs in a 5:1 stationary rectangular duct has been shown to significantly increase heat transfer at low Reynolds numbers.[13–15] However, these studies were limited to two-dimensional rectangular channel geometries that are not representative of turbine blade cooling situations.

More recently, Hibbs et al.[16] have presented the effects of the vortex generator in a stationary two-pass ribbed square coolant channel that is more representative of blade cooling. At $Re = 5 \times 10^3$, they had reported enhancements in the surface heat transfer induced by the presence of the vortex generators. However, the study of Hibbs et al.[16] was limited to stationary-blade conditions. The present paper extends this earlier study to rotating situations of interest and relevance to the gas turbine industry.

The present study uses a mass-transfer (naphthalene sublimnation) technique in view of the convenience of using this technique under conditions of rotation. The heat/mass transfer analogy can then be used to deduce the corresponding heat transfer behavior. Heat transfer measurements, under conditions of rotation, are considerably more complex because they require the use of slip rings.

Received 17 March 2000; revision received 1 November 2000; accepted for publication 3 November 2000.

*Graduate Student, Mechanical Engineering Department.
†Associate Professor, Mechanical Engineering Department. Member AIAA.
‡L. R. Daniel Professor, Mechanical Engineering Department. Member AIAA.

Furthermore, they only provide limited and rather sparse resolution, whereas the naphthalene sublimation technique provides very detailed surface resolution. The naphthalene sublimation technique, together with the heat/mass transfer analogy, has been widely used, and a recent review of mass/heat transfer measurements using this technique has been reported by Goldstein and Cho.[17] A few papers have recently been reported where the naphthalene sublimation technique has been successfully used under conditions of rotation, including those of Hibbs et al.[16] and Park and Lau.[18]

Experimental Facility and Methods

A rotating test facility is used to simulate the flow in serpentine blade-cooling ducts. This facility covers a wide range of rotation Ro and Reynolds Re numbers. The product of these parameters ($RoRe$) can be varied continuously between 0 and 25,000. The highest value can be achieved at 550 rpm by pressurizing the flow to 150 psig.

A schematic of the experimental flow loop used during this study is shown in Fig. 1. This consists of an open airflow loop connected to the test section and instrumented for flow rate, pressure, and temperature measurement of the airstream. Compressed air is supplied at a steady pressure through a pressure regulator. Test section pressure and flow control is achieved by means of ball valves placed downstream of the test section. Mass flow rate was measured in the meter run using a concentric bore orifice plate that is secured with orifice flanges. Freestream flow temperature was measured with a liquid-in-glass thermometer that has a readability of 0.25°C.

The test section, which is an analog of a two-pass coolant channel and is schematically shown in Fig. 2, consists of two 356-mm-(14-in.-) long ducts of square cross section (25.4 × 25.4 mm, or 1 × 1 in.) connected by a 180-deg bend with a short radius of 16.5 mm (0.65 in.) and a long radius of 42 mm (1.65 in.) The flow enters and leaves the test section through conically shaped transition sections. These sections provide for the transition from the circular cross section of the supply duct to the square test section cross section and are quite short in length. Note that other than these transition sections, no attempt to condition the flow is made. The flow is directed outward (toward the bend and away from the axis of rotation) in one duct and inward in the other after going around the bend. Details of the experimental facility can be found in Ref. 19.

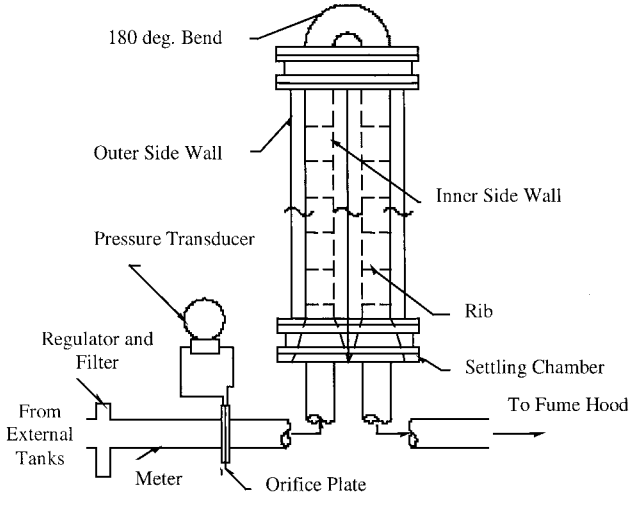

Fig. 1 Schematic of the flow loop and test section.

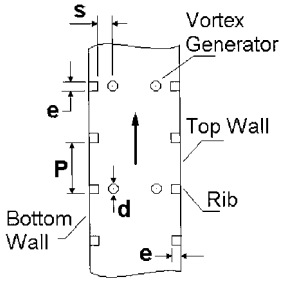

Fig. 2 Schematic of ribbed duct with vortex generators.

As noted earlier, heat transfer results in this study are deduced from the naphthalene sublimation mass-transfer technique. The test section consists of an aluminum frame that carries eight, 305-mm (12-in.) removable plates that form its inner walls. Each plate provides a reinforced recessed frame to accommodate casting of a naphthalene layer for mass-transfer measurements. Casting of the test section wall plates is done against highly polished stainless steel plates to provide a smooth and flat naphthalene reference surface.

Straight aluminum rib turbulators 25.4 mm (1.0 in.) long and with a 2.54 × 2.54 mm (0.1 × 0.1 in.) square cross section (rib side $e = 0.1$) are placed at equal streamwise increments P on the top and bottom plates and at 90 deg with respect to the flow direction for the ribbed channel studies (Fig. 2). The ribs are not coated with naphthalene and, therefore, do not participate in the mass/heat transfer process.

The vortex generators are steel rods with diameter-to-rib height ratio $d/e = 0.78$ and vortex generator to rib spacing $s/e = 0.55$. The side walls have holes of the same diameter as the vortex generator so that the latter can slide in through these holes. The vortex generators are placed directly above the rib, as shown in Fig. 2, at the proper position and at a pitch-to-rib height $P/e = 21$. Leading and trailing walls are then fastened into place. Note that we have also used a higher $s/e = 1.5$ during our study, which did not yield results as promising as $s/e = 0.55$.

The naphthalene sublimation technique requires detailed measurements of the naphthalene surface profiles for each wall plate of the test section. A computer-driven profilometer is used in this study to obtain high-resolution maps of the naphthalene surface on a predefined grid and measure the sublimation depth. The uncertainty of this measurement is of the order of 3.8 μm (0.00015 in.), and the positioning uncertainty is of the order of ±7.6 μm (±0.0003 in.). Typical grid sizes were 840 points (30 × 28) for an interrib cell with the smallest pitch, $P/e = 10.5$. The spatial resolution in the streamwise direction was 3.8 pts/e (pts/e denoting points per rib height e) and 4 pts/e in the spanwise direction. The naphthalene surface profiles for each wall were measured before and after each test. The difference between the normalized profiles gives the local sublimation depth δ. The local sublimation mass flux $\dot{m}''$ at each location is calculated as $\dot{m}'' = \rho_s \delta/\Delta t$, where ρ_s is the density of solid naphthalene and Δt is the duration of the experiment. Vapor pressure at the wall p_w is calculated from Sogin and Providence's[20] equation, $\log_{10}(p_w) = A - B/T_w$, where A and B are constants (with values of 11.884 and 6713, respectively), and T_w is the absolute wall temperature. Wall vapor density ρ_w is then calculated using the perfect gas law. Bulk vapor density of naphthalene $\rho_b(x)$ was calculated by integrating the mass flow rates of naphthalene from the inlet ($x = 0$) to the streamwise location x over the four active walls. The sublimation data from the duct centerline were used for this calculation. The bulk vapor density is assumed zero at the inlet and constant through the inactive bend. The local dimensionless mass transfer rate or Sherwood number Sh was calculated as

$$Sh = \frac{h_m D_h}{\mathcal{D}_{n-a}} = \left\{\frac{\dot{m}''}{[\rho_w - \rho_b(x)]}\right\}\frac{D_h}{D_{n-a}} = \left\{\frac{\dot{m}''}{[\rho_w - \rho_b(x)]}\right\}\frac{D_h}{\nu/Sc} \tag{1}$$

where D_h is the hydraulic diameter of the test section, h_m is the local mass-transfer convection coefficient, $\mathcal{D}_{n-a}$ is the binary diffusion coefficient for naphthalene sublimation in air, ν is the kinematic viscosity of air, and $Sc = 2.5$ is the Schmidt number for naphthalene/air.

Heat transfer results can be deduced from the mass-transfer results through the heat/mass transfer analogy,[20] $Nu = Sh(Pr/Sc)^{0.4}$, where Nu is the Nusselt number and Pr is the Prandtl number of air. The analogy is implicit in all consequent discussions of the experimental results where the Sherwood number is mentioned.

Uncertainty estimates for all computed values were computed using the second-power equation method.[21] The estimates for these experiments are comparable to previously reported values for both

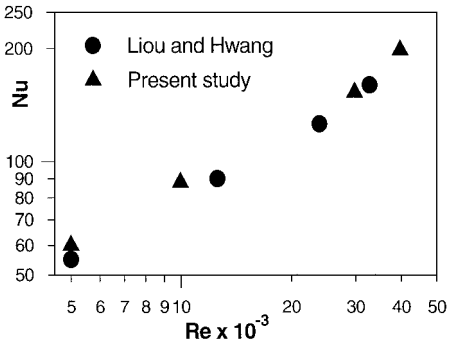

Fig. 3 Comparison of average Nusselt numbers as a function of Reynolds number from the present study in a ribbed channel, with *e/Dh* = 0.1 and *P/e* = 10.5, with those of Liou and Hwang.[26]

heat transfer and mass-transfer studies, but are believed to be conservative. Volume flow rate and duct Reynolds number uncertainties were estimated to be less than 10% for $Re > 6 \times 10^3$. Sublimation depths were maintained roughly at an average of about 254 μm (0.01 in.) by varying the duration of the experiment. This target depth was selected to minimize uncertainties in both depth measurement and changes in duct cross-sectional area. These uncertainties were found to be 1 and 3%, respectively. The resulting experimental duration was between 90 min for $Re = 3 \times 10^4$ and 180 min for $Re = 5 \times 10^3$. Vapor density uncertainty based on measured quantities is negligible for both wall and bulk values. Overall uncertainty in Sherwood number calculation is about 8% and varies slightly with Reynolds number (<1%). The uncertainty in Reynolds number is 8 and 10% in rotation number.

We have compared our naphthalene sublimation results with three past mass-transfer-based studies[22–24] as well as two previous heat transfer studies.[25,26] These comparisons have been documented by Chen et al.[27] The agreement between our measurements and all of these other studies was, in general, very good (within experimental uncertainty). We are presenting here only a representative case in Fig. 3, where our data are compared with measurements of average Nusselt numbers obtained with a laser holographic interferometric technique by Liou and Hwang[26] in a ribbed duct at various Reynolds numbers. Successful comparisons of our rotating channel naphthalene sublimation results with rotating channel heat transfer results have been presented by Acharya et al.[28]

Results and Discussion

High-resolution experimental mass-transfer results for the ribbed, two-pass, square channels with cylindrical vortex generators under stationary and rotating conditions are presented in the following sections. These results are compared to those for the corresponding channels with ribs only. The experiments were performed at $Re = 5 \times 10^3$, 1×10^4, 2×10^4, and 3×10^4 and $Ro = 0.0, 0.1, 0.2$, and 0.3 for both rib-only and rib-rod vortex generator geometries. The data are primarily presented in terms of cell-averaged Sherwood number ratios, Sh/Sh_0, for each side of the inlet and outlet channels as functions of Re and Ro. The reference Sherwood number Sh_0 is that for smooth stationary channels, as obtained from the McAdams[29] correlation. The cell averages were computed for periodically fully developed cells. The detailed mass-transfer distributions over these fully-developed cells and the first cell after the 180-deg bend are presented and discussed for selected cases of low (5×10^3) and high (3×10^4) Reynolds numbers and zero and high (0.3) Ro. Note that when complex flow turbulator geometries are used, the generated local three-dimensional flows aid in reducing the memory of the initial condition (e.g., inlet channel entrance nonuniformity, bend effect) and lead to a qualitative quasi-periodic, quasi-steady state, not more than two to three rib pitches from the location where the initial condition is imposed. This was confirmed by comparing the results from geometrically identical interrib modules in this region. Results presented in a module inside this fully developed region are representative of the qualitative mass-transfer behavior in the majority of the channel and are of principal interest to the internal blade cooling application that motivates this study. The local two-dimensional mass-transfer characteristics, which result from the complex flowfield in the ribbed ducts with vortex generators, will be discussed in the context of known local flow features such as Coriolis-induced secondary flows, recirculation regions, and wake regions (see Ref. 30). Such interpretations are realistic in regions where a single flow feature appears to dominate, whereas regions of strong interaction between secondary flow mechanisms cannot support unambiguous interpretation in the absence of local flow measurements.

In the discussions that follow, the walls of the duct referred to as stabilized are the leading and trailing walls in the inlet and outlet duct, respectively, and those referred to as destabilized are the trailing and leading ones in the inlet and outlet duct, respectively.

Averaged Mass-Transfer Data

The dependence of the cell-averaged Sherwood number ratio Sh/Sh_0 on the rotation number Ro is shown in the first row of graphs of Fig. 4 for the highest Reynolds number, $Re = 3 \times 10^4$. The second row of graphs of Fig. 4 show the dependence of the cell-averaged Sherwood number ratio Sh/Sh_0 on the Reynolds number for $Ro = 0.3$. The first two columns of graphs in Fig. 4 refer to the inlet duct (flow direction is away from the axis of rotation), and the last two rows refer to the outlet duct (flow direction toward the axis of rotation). Both the baseline rib-only (denoted as RO in Fig. 4) and rib-vortex generator (RO + VG in Fig. 4) cases are presented.

Rotation Number Effects at High Reynolds Number

At $Ro = 0.0$ (stationary case) a slight difference in mass-transfer ratios is observed between the leading and trailing walls in the inlet duct for the baseline case. This can be attributed to an asymmetry in the inlet flow profile. A small asymmetry can also be seen on the side walls of the outlet duct, possibly due to the remains of the secondary flows induced by the bend, which tend to drive the flow outward. The rest of the walls show the expected symmetry under nonrotating conditions.

For the baseline (rib-only) case, the Sherwood number ratio along both the leading and trailing walls of the inlet duct increase monotonically up to $Ro = 0.2$. The trailing wall displays higher mass-transfer ratios than the leading wall, as expected, due to the Coriolis-induced secondary flows that drive cooler mainstream flow toward the trailing side of the inlet duct. The Coriolis forces also tend to destabilize the shear layer or boundary layer along the trailing edge and stabilize it along the leading edge. Between $Ro = 0.2$ and 0.3, the ratio along the trailing wall ratio continues to increase, but at a lower rate, whereas the ratio along the leading wall decreases. The exact opposite phenomenon is observed in the outlet duct, where the leading wall ratio increases with Ro, and the trailing wall ratio reaches a peak at $Ro = 0.2$ and then decreases sharply. The leading wall displays higher mass-transfer ratios than the trailing wall, again due to the Coriolis-induced secondary flows and the destabilizing/stabilizing effects along the leading/trailing surfaces of the outlet duct.

Based on the observations outlined, it appears that for the leading wall in the inlet duct and the trailing wall in the outlet duct a somewhat anomalous or nonmonotonic behavior exists across $Ro = 0.2$. Strong evidence of this nonmonotonic behavior also exists in the distributions of the Sherwood number ratio along the side walls. Again, for the baseline (rib-only) case, the mass-transfer ratio along both side walls in the inlet duct grows monotonically up to $Ro = 0.2$. Beyond that point, the outer wall ratio declines whereas the inner wall ratio continues to increase. Furthermore, the relative magnitudes of outer and inner wall mass-transfer ratios change sign from $Ro = 0.2$ (outer higher than inner) to $Ro = 0.3$ (inner higher than outer). The exact same qualitative trend is observed for the side walls of the outlet duct. To confirm the nonmonotonic behavior observed, the experiments were repeated several times, and the observed trends were always repeatable. Therefore, there is a high degree of confidence that the nonmonotonic behavior observed across $Ro = 0.2$ is indeed real. In examining the published data, as in the present

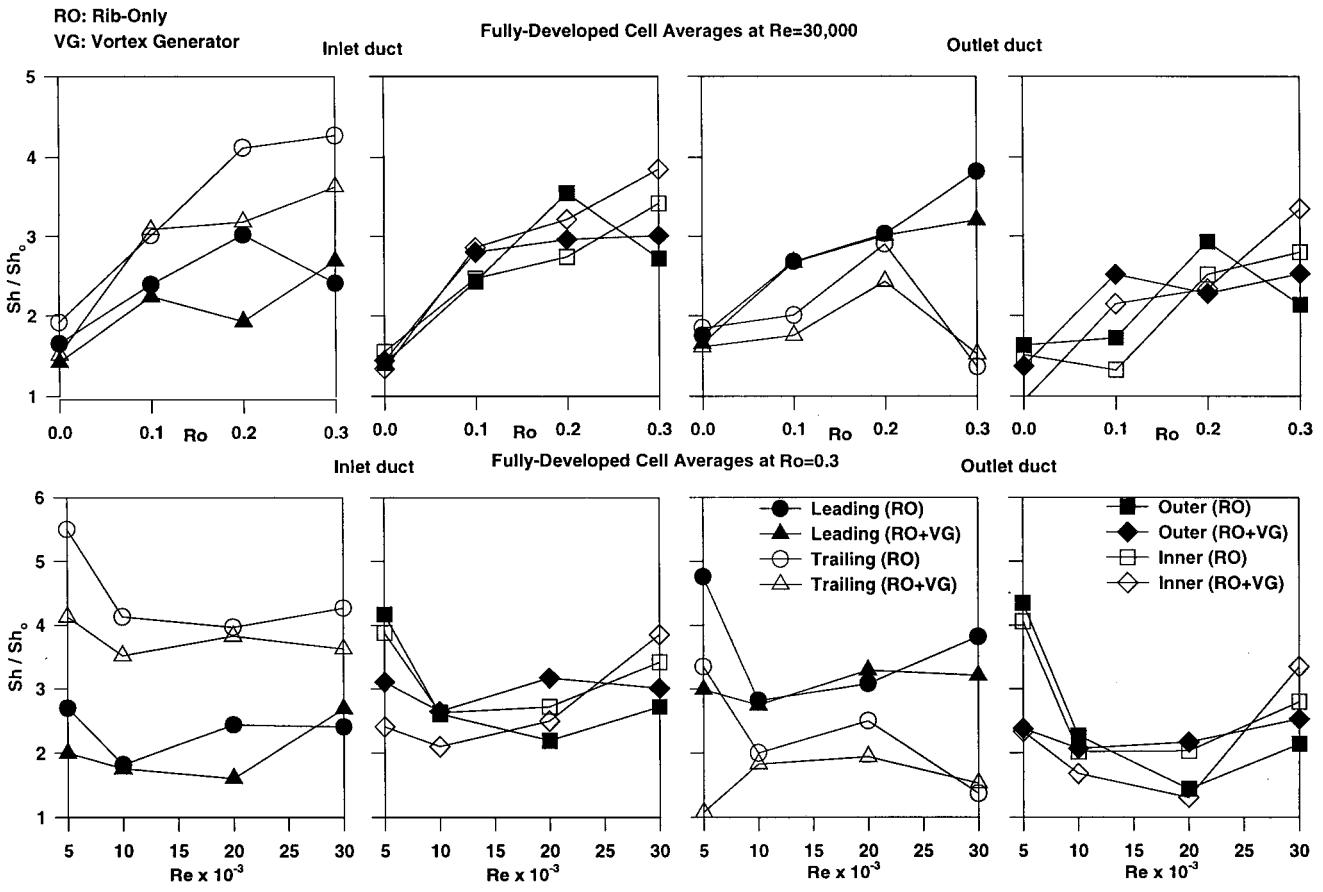

Fig. 4 Fully developed cell averages of Sherwood number ratios Sh/Sh_0 at different rotation Ro and Reynolds Re numbers ($P/e = 10.5$, $e/D_h = 0.1$, $d/e = 0.78$, and $s/e = 0.55$).

study, the behavior along the leading edge of the inlet duct and that along the trailing edge of the outlet duct have been reported to be more complex than that along the opposite surfaces. Nonmonotonic behavior with increasing Ro has been reported with an initial decrease followed by an increase due to centrifugal buoyancy,[31] as well as an initial increase followed by a decrease due to changes in the flow pattern.[32] In the absence of flow data and the measured details of the complex strongly three-dimensional flowfield, only a speculative explanation can be given at this time. The change in behavior observed across $Ro = 0.2$ is related to a change in the nature of the secondary flows in the duct. At low rotation numbers, the Coriolis-induced secondary flows may still be competing with the secondary flows induced by the turbulent stresses in the noncircular channel. Coriolis forces may augment stress anisotropies, which, in turn, may enhance the stress-driven secondary flows and, thus, promote the surface mass transfer. At high rotation numbers this competition may be clearly in favor of the Coriolis-induced secondary flows that lead to a reduction of mass transfer along the stabilized surface (leading surface along the inlet and trailing surface along the outlet). This competitive mechanism may also be responsible for the overall enhancement of mass (heat) transfer observed with increasing rotation number, particularly in the range 0–0.2. To examine the dependence of mass transfer on Ro, we have computed four-wall averages combining data from both inlet and outlet channels in the fully developed region. We found that these average values of the Sherwood number ratio have a relatively weak dependence on Reynolds number within the range of our experiments for $Re > 5 \times 10^3$. We also found that the dependence of Sherwood number ratio on Ro number is of the form $a + bRo^{0.51}$. This was so both for the rib-only case and the one with vortex generators; each case yields different constants a and b of similar order of magnitude. The data we have are rather limited, to yield reliable constants. However, note that the dependence of the Sherwood number ratio on Ro is approximately a square-root one.

Although the qualitative trends of the rotation number dependence are similar between inlet and outlet ducts, quantitative differences are observed. These differences can be attributed to a long-lasting effect of the bend and the reversal of the flow direction. Essentially, the spatial distributions of the flow-field initial conditions for the inlet and outlet ducts are quite different.

The anomalous nonmonotonic behavior noted earlier seems to be reinforced by the results of the case where vortex generators are used. The presence of the vortex generators is certainly capable of influencing the details of the secondary flows in the channel. Thus, qualitative changes should be expected and are observed. For instance, in the inlet duct at low Ro (<0.1), the presence of the vortex generators influences the mass-transfer ratio very little. However, at high Ro (≥ 0.2), the effect is substantial, resulting in degradation of mass transfer and the replacement of the stabilized (leading) wall peak at $Ro = 0.2$ by a minimum. At $Ro = 0.3$ the destabilized (trailing) surface displays degradation, whereas the stabilized (leading) one shows enhancement, and, as a consequence, the mass-transfer rates from the leading and trailing surfaces are closer to each other with vortex generators. This may be due to the disruption of the rotation-induced secondary flows by the presence of the vortex generators. Along the outlet duct also, the differences in mass transfer between the leading and trailing surfaces are lower at $Ro = 0.3$. The side walls mostly display mass-transfer enhancement when vortex generators are included, with the exception of the $Ro = 0.2$ case where enhancement is observed only along the inner wall. Again, the presence of an anomalous behavior at the neighborhood of $Ro = 0.2$ points toward the existence of a threshold condition.

Reynolds Number Effects at High Rotation Number

It is seen from the bottom row of graphs on Fig. 4 that the effect of the Reynolds number on the mass-transfer ratio is significant at low Reynolds numbers for the baseline (rib-only) case. All sides of both ducts display a sharp decrease in mass-transfer ratio between

$Re = 5 \times 10^3$ and 1×10^4. Note that it is the mass-transfer ratio (normalized with respect to the smooth channel correlation) that decreases with Reynolds number and not the mass transfer itself, indicating that the ribbed duct has a weaker dependence on the Reynolds number than the normalizing smooth channel correlation. At higher Reynolds number, the Sherwood number ratios tend to increase again.

The Reynolds number dependence of the rib-rod case appears to be considerably weaker than the rib-only case. Severe mass transfer degradation is experienced at low Reynolds numbers for all sides of both inlet and outlet ducts. Enhancement is observed as the Reynolds number increases, particularly for the side walls. At the highest Reynolds number, some enhancement is seen on the stabilized walls of the inlet and outlet ducts.

Comparison Between Rib-Rod and Rib-Only Results

Table 1 gives a comparison between the rib-rod case and the rib-only at $Re = 3 \times 10^4$ and with Ro varying from 0.0 to 0.3 at 0.1 intervals. The comparison was made by averaging the two consecutive periodically fully developed cells. As can be observed, mass transfer enhancement is achieved by the use of vortex generators on the stabilized walls for the highest rotation number only, while degradation occurs on the destabilized walls. The side walls show enhancement at Ro of 0.1 and 0.3.

In Table 2 the comparison is made for fixed $Ro = 0.3$ and varying Reynolds number from 5×10^3 to 3×10^4. Degradation is observed on all walls at low Reynolds numbers. This degradation decreases with increasing Reynolds number. At the highest, $Re = 3 \times 10^4$, enhancement can be reported in all walls except those destabilized by rotation.

The results seem to imply that the performance of vortex generators in improving mass transfer becomes better as both the Reynolds and rotation numbers are increased.

Detailed Mass-Transfer Distributions

Figures 5–8 show detailed Sherwood number ratio results in the form of constant Sherwood number ratio contours. These are presented in Figs. 5–8 for two fully developed cells in the inlet duct, the cell following the 180-deg bend, and a pair of two fully developed cells in the outlet duct. When analyzing Figs. 5–8, note that the vortex generators are placed on alternate ribs and that in the pair of fully developed cells shown, there is no vortex-generator upstream of the first cell, whereas there is a vortex generator upstream of the second cell. The contours in Figs. 5 and 7 are for the baseline case without vortex generators (henceforth referred to as rib-only cases). High Reynolds number stationary results ($Re = 3 \times 10^4$, $Ro = 0.0$) are shown in Fig. 5, and high Reynolds number with rotation results ($Re = 3 \times 10^4$, $Ro = 0.3$) are presented in Fig. 7. The rib-only

Table 1 Fully developed cell average comparison between rib-rod vortex generator and rib-only baseline measurement at $Re = 3 \times 10^4$, $s/e = 0.55$, $P/e = 10.5$, $e/D_h = 0.1$, and $d/e = 0.78$

	$Ro = 0.0$		$Ro = 0.1$		$Ro = 0.2$		$Ro = 0.3$	
Wall no.	Inlet	Outlet	Inlet	Outlet	Inlet	Outlet	Inlet	Outlet
Leading	0.86	0.94	0.94	1	0.64	1	1.12	0.84
Trailing	0.79	0.87	1.03	0.88	0.77	0.84	0.85	1.12
Outer	1.02	0.84	1.15	1.46	0.83	0.77	1.11	1.18
Inner	0.87	0.63	1.16	1.62	1.17	0.93	1.13	1.2

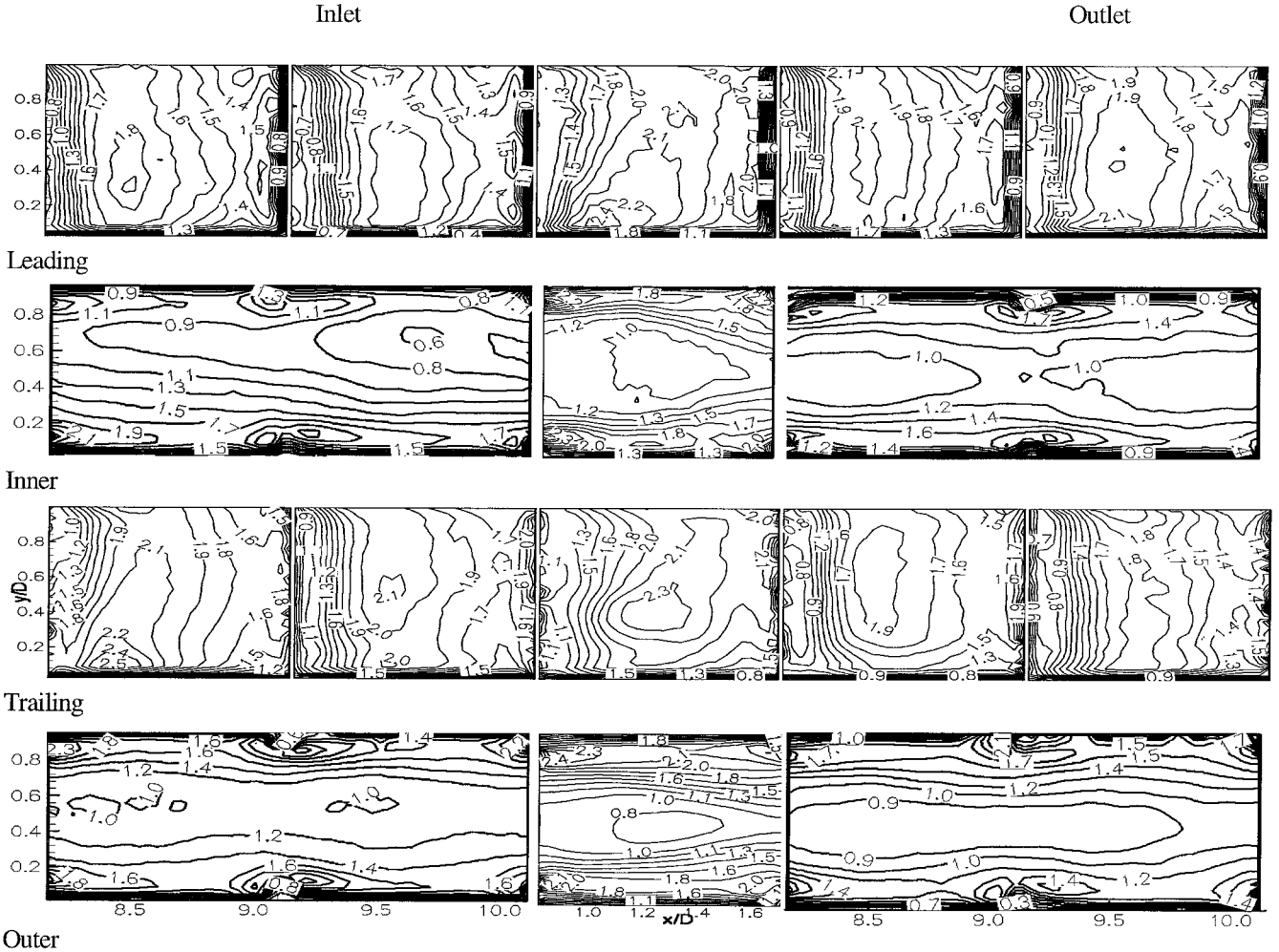

Fig. 5 Detailed Sherwood number ratio distributions Sh/Sh_0 in selected developing and fully developed regions for the ribbed duct at $Re = 3 \times 10^4$, $Ro = 0.0$, $P/e = 10.5$, and $e/D_h = 0.1$.

Table 2 Fully developed cell average comparison between rib-rod vortex generator and rib-only baseline measurement at $Ro = 0.3$, $s/e = 0.55$, $P/e = 10.5$, $e/D_h = 0.1$, and $d/e = 0.78$

	$Re = 5 \times 10^3$		$Re = 1 \times 10^4$		$Re = 2 \times 10^4$		$Re = 3 \times 10^4$	
Wall no.	Inlet	Outlet	Inlet	Outlet	Inlet	Outlet	Inlet	Outlet
Leading	0.74	0.63	0.97	0.98	0.66	1.07	1.12	0.84
Trailing	0.75	0.32	0.85	0.92	0.97	0.78	0.85	1.12
Outer	0.75	0.55	1.02	0.91	1.45	1.51	1.11	1.18
Inner	0.62	0.57	0.8	0.83	0.92	0.65	1.13	1.2

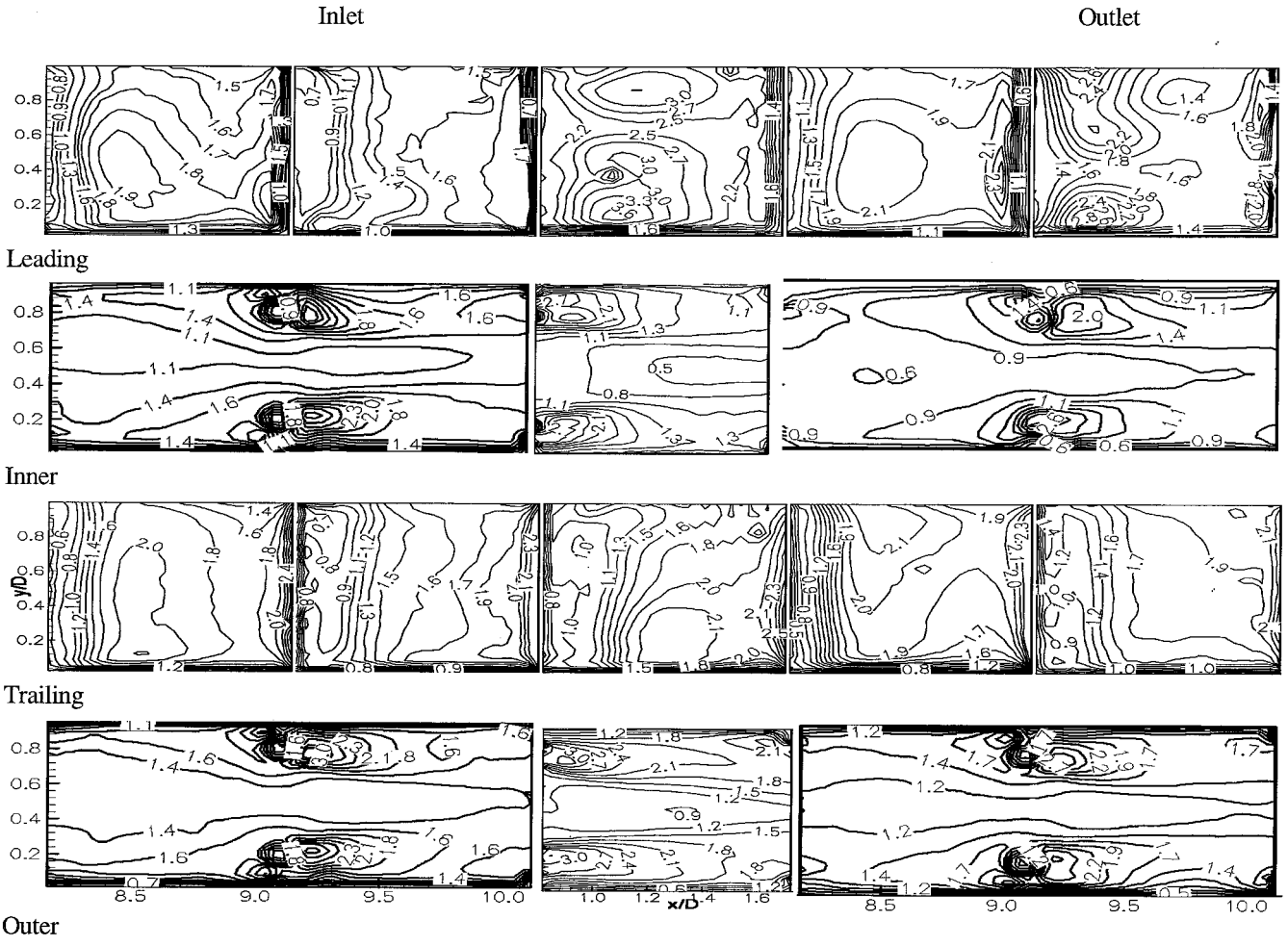

Fig. 6 Detailed Sherwood number ratio distributions Sh/Sh_0 in selected developing and fully developed regions for the ribbed duct with horizontal rod vortex generators at $Re = 3 \times 10^4$, $Ro = 0.0$, $s/e = 0.55$, $P/e = 10.5$, $e/D_h = 0.1$, and $d/e = 0.78$.

results are included here as a baseline case to compare with the corresponding cases where vortex generators were present (henceforth referred to as rib-rod cases). The detailed Sherwood number ratio results in the form of constant Sherwood number ratio contours for these cases are presented in Figs. 6 and 8.

Comparison between Figs. 5 and 6, for the stationary case, indicate that the major effect of the presence of vortex generators is one similar to that produced by a higher rib. It is most likely that the flow between rib and rod is inhibited, leading to this behavior. It is evident, by comparing the second fully developed cell of the leading and trailing surfaces in both the inlet and outlet duct, that peak mass transfer in the interrib module occurs closer to the downstream rib, and the reattachment location behind the ribs with vortex generators has been pushed downstream and probably straddles the next rib. The same evidence exists in the after-bend module in the outlet duct. Indeed, a region of maximum mass transfer indicative of reattachment is visible in the rib-only case, whereas it is absent in the rib-rod case. This is the main reason why the rib-rod case fails to produce mass-transfer enhancement in this module. The absence of reattachment behind the vortex-generator bearing rib is also visible on the side walls of the corresponding module. The wake regions behind the vortex-generator bearing ribs are considerably larger in the rib-rod case extending closer to the downstream rib. This wake region manifests itself as a single structure, indicating that flow through the gap between the rib and the vortex generator is very weak, if nonexistent. The same can be deduced by the signature of a single recirculation zone on the side walls ahead of the vortex-generator bearing rib. Considerable enhancement is observed behind the vortex-generator bearing ribs both in the larger wake region and the central region of the wall. The latter region is enhanced, probably due to the acceleration of the mean flow caused by the increased blockage, as well as by the turbulence enhancement caused by the presence of the vortex generator. Note that the mass transfer distribution on the side walls is strongly nonuniform in the cross-stream direction. Therefore, drawing conclusions regarding overall mass transfer from centerline surveys could be misleading. This is true for the stationary case examined here, as well as the rotating case presented later.

In the module upstream of the vortex generator, the maximum in the mass-transfer ratio associated with reattachment can be clearly

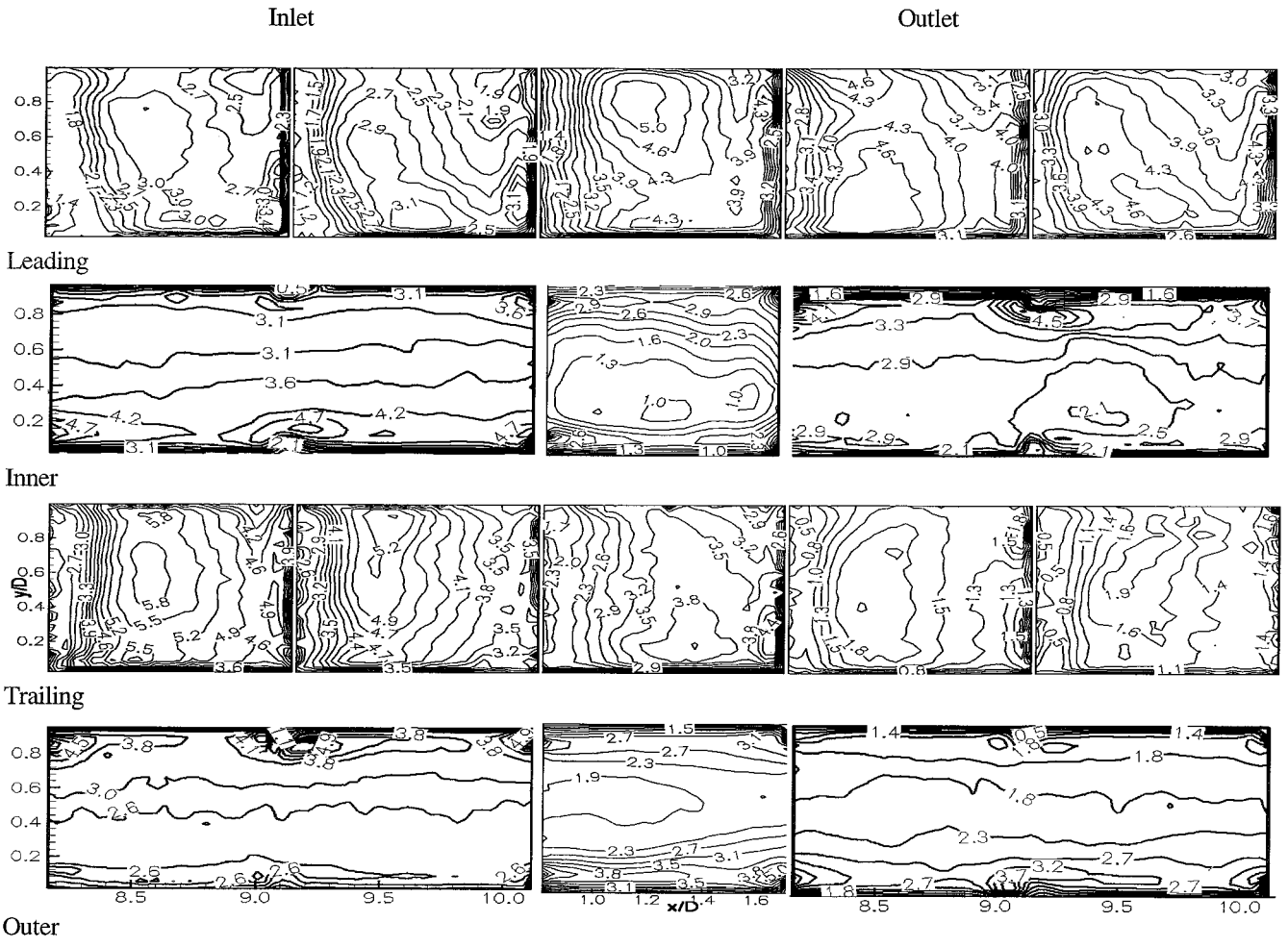

Fig. 7 Detailed Sherwood number ratio distributions Sh/Sh_0 in selected developing and fully developed regions for the ribbed duct at $Re = 3 \times 10^4$, $Ro = 0.3$, $P/e = 10.5$, and $e/D_h = 0.1$.

observed for both the leading and trailing walls of the inlet and outlet ducts. Thus, the general nature of the flow pattern in this upstream module is comparable with that in a rib-only module case. However, there are observable differences in the patterns and in the magnitudes between the rib-rod and rib-only cases, and these are consequences of the vortex generator located in the previous module. For the side walls ahead of the vortex-generator bearing rib, the rib-rod case shows significant enhancement in this region. This is most likely due to increased turbulent intensity introduced by the vortex generator upstream that is transported downstream. In the module after the bend, the bend effects that induce secondary flow from the inner to the outer surface can be observed. These effects seem to be more prominent for the rib-rod case, where the Sherwood number ratio on the outer wall is higher than that along the inner wall.

Figures 7 and 8 present the detailed mass-transfer ratio data for the rotating cases and show the basic features of the Coriolis effect. For both rib-only and rib-rod cases, the stabilized wall is subject to lower mass-transfer ratios than the destabilized wall. The same signature exists on the side walls. The half of the side wall toward the stabilized side has lower mass-transfer ratios than the other half adjacent to the destabilized wall. In the shear-layer regions behind the ribs and in the wakes of the vortex generators, the Coriolis effect leads to substantially diminished Sherwood number ratios on the stabilized wall side and substantially enhanced ratios on the destabilized side.

The same salient features as for the stationary cases are observed in terms of the rib and vortex-generator effects. In addition, it is observed that on the walls destabilized by the effect of rotation, degradation (relative to the rib-only case) occurs immediately after the vortex-generator bearing rib. This is followed by an increase in mass transfer leading to enhancement before the downstream rib (with no vortex generator). The module after the no-generator rib shows predominantly degradation relative to the rib-only case. On the stabilized walls, the presence of the vortex generators leads to modest mass-transfer enhancement downstream of the rib-rod element in the majority of the intrarib space. This enhancement is also sustained downstream of the plain rib as well. It can be concluded from this consistent and periodic pattern at high Reynolds and Ro numbers that the presence of the vortex generators favors the stabilized walls, whereas it is detrimental to the destabilized walls of the rotating coolant channel. As a result, the differences in heat transfer between the leading and trailing walls are smaller in the presence of vortex generators. The comparison between the rib-only and rib-rod cases also shows that in the module after the vortex-generator bearing rib, the presence of the vortex generators seem to reduce the asymmetry between leading and trailing walls caused by the Coriolis effect. This is also indicated by the averaged data in Fig. 4 and can be attributed to the possible disruption, caused by the vortex generators, of the secondary flows induced by rotation. In the module after the bend, the general trends, caused by the presence of the bend, that have been discussed in the previous section are present in the rib-only case. In the rib-rod case (Fig. 8) a vortex generator exists over the first rib after the bend. Its presence dominates in defining the qualitative features of the mass-transfer distribution. However, the bend effect is still visible by virtue of the asymmetry between the outer and inner walls. The outer wall shows higher overall mass transfer than the inner one. Also, the strong asymmetry between leading and trailing walls perpetrated by Coriolis effects and observed in the after-bend module for the rib-only case is absent in the rib-rod case. This can be attributed to the presence of the vortex generator, which may disrupt the local secondary flow patterns emerging from the bend. Also note that the minimum in mass-transfer ratio observed in the central region of

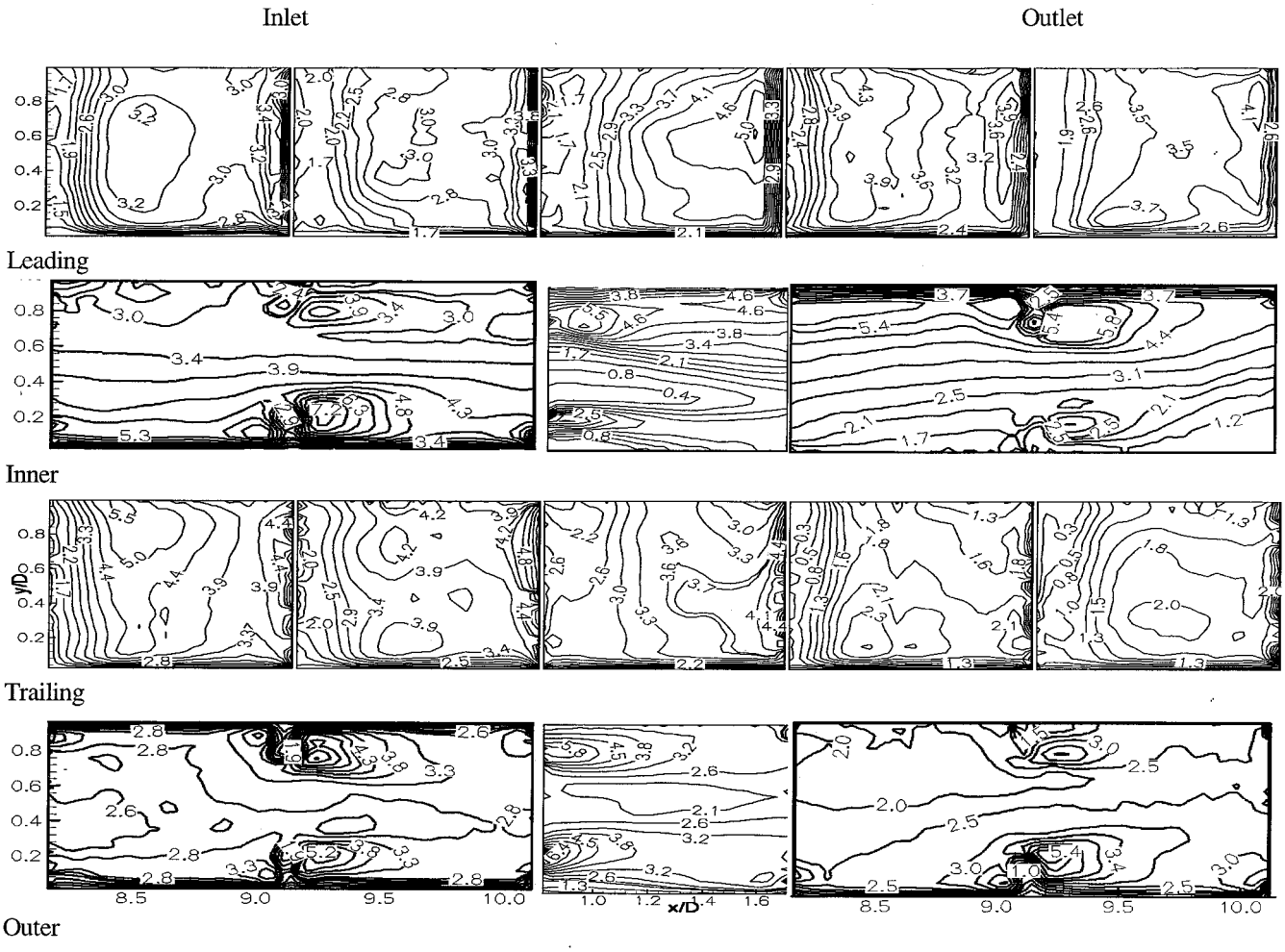

Fig. 8 Detailed Sherwood number ratio distributions Sh/Sh_0 in selected developing and fully developed regions for the ribbed duct with horizontal rod vortex generators at $Re = 3 \times 10^4$, $Ro = 0.3$, $s/e = 0.55$, $P/e = 10.5$, $e/D_h = 0.1$, and $d/e = 0.78$.

the inner wall after the bend is considerably smaller when vortex generators are present (approximately 0.4 in the rib-rod case rather than 1 for the rib-only case).

The qualitative features discussed for the high Reynolds number case with rotation are essentially the same at low Reynolds number under the same rotation number.

Concluding Remarks

High-resolution experimental mass-transfer results for ribbed, two-pass, square channels with cylindrical vortex generators under stationary and rotating conditions have been presented and discussed. These results have been compared to those for the corresponding channels with ribs only. Based on the discussion and comparisons of these results the following conclusions can be drawn:

1) When placed directly above the ribs, vortex generators seem to produce results that would be expected from a taller rib. Effects of flow through the gap between the vortex generator and the rib do not seem to be present.

2) The Coriolis effect is dominant in all rotating cases. The presence of vortex generators tends to reduce the asymmetry caused by rotation between stabilized and destabilized walls.

3) Vortex generators appear to be effective at high Reynolds and rotation numbers.

4) The results with vortex generators indicate that the mass transfer in the ducts is less sensitive to the Reynolds number compared to the rib-only duct.

5) The vortex generators cause severe mass-transfer degradation at low Reynolds and rotation numbers.

6) Vortex generators are more effective in enhancing mass transfer on the side walls of the ducts.

7) Vortex generator use may be more effective on the stabilized walls of the rotating ducts.

Acknowledgments

This research was performed under a subcontract from the South Carolina Energy Research and Development Center to Louisiana State University (93-01-SR015). The contract monitors were Daniel Fant and Larry Golan. Their help is gratefully acknowledged.

References

[1] Acharya, S., Myrum, T., and Inamdar, S., "Effect of Subharmonic Flow Pulsation in a Ribbed Pipe: Flow Visualization and Pressure Measurements," *AIAA Journal*, Vol. 29, No. 9, 1991, pp. 1390–1400.

[2] Han, J. C., and Zhang, P., "Effect of Rib-Angle Orientation on Local Mass Transfer Distribution in a Three-Pass Rib-Roughened Channel," *Journal of Turbomachinery*, Vol. 113, No. 1, 1991, pp. 123–130.

[3] Acharya, S., Dutta, S., Myrum, T., and Baker, R. S., "Periodically Developed Flow and Heat Transfer in a Ribbed Duct," *International Journal of Heat and Mass Transfer*, Vol. 36, No. 8, 1993, pp. 2069–2082.

[4] Abuaf, N., and Kercher, D. M., "Heat Transfer and Turbulence in a Turbulated Blade Cooling Circuit," *Journal of Turbomachinery*, Vol. 116, No. 3, 1994, pp. 169–177.

[5] Acharya, S., Myrum, T., Sinha, S., and Qiu, X., "Developing and Periodically Developed Flow, Temperature and Heat Transfer in a Ribbed Duct," *International Journal of Heat Mass Transfer*, Vol. 40, No. 2, 1997, pp. 461–480.

[6] Acharya, S., Myrum, T. A., and Dutta, S., "Heat Transfer in Turbulent Flow Past a Surface-Mounted Two-Dimensional Rib," *Journal of Heat Transfer*, Vol. 120, No. 3, 1998, pp. 550–562.

[7] Taslim, M. E., Li, T., and Spring, S. D., "Measurements of Heat Transfer Coefficients and Friction Factors in Passages Rib-Roughened on All Walls," *Journal of Turbomachinery*, Vol. 120, No. 3, 1998, pp. 575–581.

[8]Acharya, S., Dutta, S., Myrum, T., and Baker, R. S., "Turbulent Flow Past a Surface Mounted Rib," *Journal of Fluids Engineering*, Vol. 116, No. 2, 1994, pp. 238–246.

[9]Karniadakis, G. E., Mikic, B. B., and Patera, A. T., "Minimum-Dissipation Transport Enhancement by Flow Destabilization: Reynolds' Analogy Revisited," *Journal of Fluid Mechanics*, Vol. 192, March 1991, pp. 365–391.

[10]Wroblewski, D. E., and Eibeck, P. A., "Measurements of Turbulent Heat Transport in a Boundary Layer with an Embedded Streamwise Vortex," *International Journal of Heat and Mass Transfer*, Vol. 34, No. 7, 1991, pp. 1617–1631.

[11]Garimella, S. V., and Eibeck, P. A., "Enhancement of Single Phase Convective Heat Transfer from Protruding Elements Using Vortex Generators," *International Journal of Heat and Mass Transfer*, Vol. 34, No. 9, 1991, pp. 2431–2433.

[12]Hung, Y. H., and Lin, H. H., "An Effective Installation of Turbulence Promoters for Heat Transfer Augmentation in a Vertical Rib-Heated Channel," *International Journal of Heat and Mass Transfer*, Vol. 35, No. 1, 1992, pp. 29–42.

[13]Myrum, T. A., Acharya, S., Inamdar, S., and Mehrotra, A., "Vortex Generator Induced Heat Transfer Augmentation Past a Rib in a Heated Duct Air Flow," *Journal of Heat Transfer*, Vol. 114, 1992, pp. 280–284.

[14]Myrum, T. A., Qiu, X., and Acharya, S., "Heat Transfer Enhancement in a Ribbed Duct Using Vortex Generators," *International Journal of Heat and Mass Transfer*, Vol. 36, No. 14, 1993, pp. 3497–3508.

[15]Myrum, T., Acharya, S., Sinha, S., and Qiu, X., "Flow and Heat Transfer in a Ribbed Duct with Vortex Generators," *Journal of Heat Transfer*, Vol. 118, No. 2, 1996, pp. 294–300.

[16]Hibbs, R., Acharya, S., Chen, Y., Nikitopoulos, D. E., and Cormier, R., "Mass Transfer Distribution in a Rotating, Two-Pass Channel with Smooth and Ribbed Walls," *Proceedings 31st ASME-National Heat Transfer Conference*, Vol. 2, HTD-324, 1996, pp. 123–136.

[17]Goldstein, R. J., and Cho, H. H., "A Review of Mass Transfer Measurements Using Napthalene Sublimation," *Experimental Thermal and Fluid Science*, Vol. 10, Jan. 1995, pp. 416–434.

[18]Park, C. W., and Lau, S. C., "Effect of Channel Orientation of Local Heat (Mass) Transfer Distributions in a Rotating Two-Pass Square Channel with Smooth Walls," *Journal of Heat Transfer*, Vol. 120, No. 3, 1998, pp. 624–632.

[19]Hibbs, G. R., "Vortex Generator Induced Heat Transfer Enhancement in Gas Turbine Coolant Channel," M.S. Thesis, Mechanical Engineering Dept., Louisiana State Univ., Baton Rouge, LA, May 1996.

[20]Sogin, H. H., and Providence, R. I., "Sublimation from Disks to Air Streams Flowing Normal to Their Surfaces," *Transactions of the American Society of Mechanical Engineers*, Vol. 80, No. 1, 1958, pp. 61–69.

[21]Kline, S. J., and McClintock, F. A., "Describing Uncertainties in Single-Sample Experiments," *Mechanical Engineering*, Vol. 75, No. 1, 1958, pp. 3–8.

[22]Kukreja, R. T., Lau, S. C., and McMillin, V. R. D., "Local Heat/Mass Transfer Distribution in a Square Channel with Full and V-Shaped Ribs," *International Journal of Heat and Mass Transfer*, Vol. 36, No. 8, 1992, pp. 2013–2020.

[23]Chyu, M. K., and Wu, L. X., "Combined Effects of Rib Angle-of-Attack and Pitch-to-Height Ratio on Mass Transfer from a Surface with Transverse Ribs," *Experimental Heat Transfer*, Vol. 2, 1989, pp. 291–308.

[24]Han, J. C., Chandra, P. R., and Lau, S. C., "Local Heat/Mass Transfer Distributions Around Sharp 180° Turns in Two-Pass Smooth and Rib-Roughened Channels," *Journal of Heat Transfer*, Vol. 110, No. 1, 1988, pp. 91–98.

[25]Han, J. C., and Park, J. S., "Developing Heat Transfer in Rectangular Channels with Rib Turbulators" *International Journal of Heat and Mass Transfer*, Vol. 31, No. 1, 1988, pp. 183–195.

[26]Liou, T. M., and Hwang, D. W., "Turbulent Heat Transfer Augmentation and Friction in Periodic Fully Developed Channel Flows," *Journal of Heat Transfer*, Vol. 114, No. 1, 1992, pp. 56–64.

[27]Chen, Y., Nikitopoulos, D. E., Hibbs, R., Acharya, S., and Myrum, T. A., "Detailed Mass Transfer Distribution in a Ribbed Coolant Passage," American Society of Mechanical Engineers, Paper 96-WA/HT-11, 1996.

[28]Acharya, S., Eliades, V., and Nikitopoulos, D. E., "Heat Transfer Enhancements in Rotating Two-Pass Coolant Channels with Profiled Ribs: Average Results," *Journal of Turbomachinery*, Vol. 23, No. 1, 2001, pp. 97–106.

[29]McAdams, W., *Heat Transmission*, 3rd. ed., McGraw–Hill, New York, 1954.

[30]Nikitopoulos, D. E., Eliades, V., and Acharya, S., "Heat Transfer Enhancements in Rotating Two-Pass Coolant Channels with Profiled Ribs: Detailed Measurements," *Journal of Turbomachinery*, Vol. 23, No. 1, 2001, pp. 107–114.

[31]Wagner, J. H., Johnson, B. V., Graziani, R. A., and Yeh, F. C., "Heat Transfer in Rotating Serpentine Passages with Trips Normal to the Flow," *Journal of Turbomachinery*, Vol. 114, No. 4, 1992, pp. 847–857.

[32]Dutta, S., Han, J.-C., and Lee, C. P., "Local Heat Transfer in a Rotating Two-Pass Ribbed Triangular Duct with Two Model Orientations," *International Journal of Heat and Mass Transfer*, Vol. 39, No. 4, 1996, pp. 707–715.